

Tracing satellite planes in the Sculptor group:

I. Discovery of three faint dwarf galaxies around NGC 253

David Martínez-Delgado^{1*}, Dmitry Makarov², Behnam Javanmardi³, Marcel S. Pawlowski⁴, Lidia Makarova²,
Giuseppe Donatiello⁵, Dustin Lang⁶, Javier Román^{1,7,8}, Kathy Vivas⁹, Julio A. Carballo-Bello¹⁰

¹ Instituto de Astrofísica de Andalucía, CSIC, E-18080 Granada, Spain

² Special Astrophysical Observatory of the Russian Academy of Sciences, Nizhniy Arkhyz, 369167, Russia

³ LESIA, Observatoire de Paris, Université PSL, CNRS, Sorbonne Université, Université de Paris, 5 place Jules Janssen, 92195 Meudon, France

⁴ Leibniz-Institut für Astrophysik Potsdam (AIP), An der Sternwarte 16, D-14482 Potsdam, Germany

⁵ UAI – Unione Astrofili Italiani /P.I. Sezione Nazionale di Ricerca Profondo Cielo, 72024 Oria, Italy

⁶ Perimeter Institute for Theoretical Physics, 31 Caroline St N, Waterloo, Canada

⁷ Instituto de Astrofísica de Canarias, c/ Vía Láctea s/n, E-38205, La Laguna, Tenerife, Spain

⁸ Departamento de Astrofísica, Universidad de La Laguna, E-38206, La Laguna, Tenerife, Spain

⁹ Cerro Tololo Inter-American Observatory, NSF's NOIRLab, Casilla 603, La Serena, Chile

¹⁰ Instituto de Alta Investigación, Sede Esmeralda, Universidad de Tarapacá, Av. Luis Emilio Recabarren 2477, Iquique, Chile

April 2021

ABSTRACT

Context. In the last years, a new generation of large-scale imaging surveys have probed for the first time wide field regions around some nearby galaxies at unprecedented low surface brightness regime ($\sim 28.0\text{--}29.0$ mag arcsec⁻²). This offers a chance of discovering very faint dwarf satellites by means of systematic visual inspection of these public deep images.

Aims. In this paper we report the first results of a systematic survey of faint dwarf spheroidal galaxies in the vicinity of the bright late-type spiral NGC 253 galaxy by means of a visual inspection of the images taken by the Dark Energy Survey.

Methods. We performed a new NGC 253 satellite search using coadded image cutouts reprocessed in the DESI Legacy imagen surveys. We used GALFIT software for the photometric and structural properties of three dwarf galaxies.

Results. Three new dwarf galaxies have been discovered in the vicinity of the brightest member of the Sculptor filament, the late-type spiral NGC 253, located at a distance of 3.7 Mpc towards Anti-Virgo. We named them Do II, Do III and Do IV. Assuming they are companions of NGC 253, their total absolute V -magnitudes fall in the -7 to -9 mag range, which is typical for dwarf satellites in the local Universe. The central surface brightness tend to be extremely low for all the discovered dwarfs and fall roughly in the range of $25\text{--}26$ mag arcsec⁻² in g -band. Using known data on distances and velocities of galaxies, we estimate the total virial mass of the NGC 253 group to be $8 \times 10^{11} M_{\odot}$, which gives the virial radius $R_{200} = 186$ kpc and the turn-around radius of 706 kpc. We also discuss the possible existence of a spatially flattened and velocity-correlated satellite system around NGC 253. This large-scale structure is orientated almost edge-on to line of sight. The possible plane of satellites is only 31 kpc thick with the minor-to-major axis ratio of 0.14. Four out of five galaxies with measured velocities follow a common velocity trend similar to those observed in the planes of satellites around the Andromeda and Centaurus A galaxies. However, the small number of galaxies with known velocities prevents to reach a definitive conclusion about the formation scenario of the structure and its possible relation to the surrounding cosmic web.

Key words. galaxies: individual: NGC253 – galaxies: formation – galaxies:dwarf – surveys

1. Introduction

Dwarf galaxies are rich laboratories for studying stellar populations (Tolstoy 2000; Grebel 2005), galaxy formation scenarios, cosmological models, and gravitational theories (Kroupa et al. 2018). The observations of dwarf galaxies in the Local Group (LG) has faced the standard Lambda-Cold-Dark-Matter (Λ CDM) cosmological model with a number of challenges (see e.g. Bullock & Boylan-Kolchin 2017, for a review). In fact, some recent observational studies indicate that the challenges to Λ CDM appear not to be limited to only the LG. Chiboucas et al. (2013) and Müller et al. (2018b) found discs of satellites around M 81 and the Centaurus A galaxy similar to those rotating around

the Milky Way (Pawlowski & Kroupa 2013) and M 31 (Ibata et al. 2013); Smercina et al. (2018) and Bennet et al. (2019) reported a *missing satellites* problem in the M 94 and M 101 groups; and Javanmardi & Kroupa (2020) found an unexpected correlation between the number of satellites and the bulge-to-total baryonic mass ratio extending beyond the LG. These findings require further deep surveys of faint dwarf galaxies around as many massive galaxies in the local volume as possible.

Λ CDM simulations predict that subhalos around more massive host halos, such as that expected to surround the Milky Way, are mostly randomly isotropically distributed and have largely uncorrelated relative velocities. While some anisotropy in distribution and some coherence in motion is expected – induced by the preferential accretion of subhalos along cosmic filaments

* Talentia Senior Fellow

and in small groups (Libeskind et al. 2011; Pawlowski et al. 2012; Shao et al. 2018) – an overall close-to-isotropic distribution of satellite systems is a robust prediction of the underlying model. This is because the positions and motions of satellites on scales of 100’s of kpc are not strongly affected by the intricacies of baryonic physics, or the minutiae of how these are implemented in cosmological simulations. Testing this prediction for the phase-space distribution of satellite galaxies has revealed a serious challenge to Λ CDM in the LG: the observed satellite galaxy systems of the Milky Way (Pawlowski & Kroupa 2013) and M 31 (Ibata et al. 2013) display flattened distributions, whose kinematics indicate a preference of satellites to co-orbit along these structures. Recent proper motion data indicate that a substantial fraction of the Milky Way satellites (Fritz et al. 2018; Li et al. 2021), as well as at least two of M 31’s on-plane satellites (Sohn et al. 2020), indeed orbit along these planes of satellite galaxies. Simulated systems with similar degrees of coherence are exceedingly rare in cosmological simulations (Ibata et al. 2014). For a review, see Pawlowski (2018).

Some similar satellite alignments have been identified outside the LG. The most prominent to date is a flattened distribution of satellites, close to an edge-on orientation, identified around Centaurus A by Tully et al. (2015). To this, Müller et al. (2018b) added evidence for line-of-sight velocity kinematics being consistent with a rotating satellite plane, a finding recently confirmed when additional spectroscopic velocity measurements brought the number of kinematically correlated satellites to 21 out of 28 (Müller et al. 2021a). Some additional hints at similar structures exist around other host galaxies such as M 81 (Chiboucas et al. 2013), as well as in a statistical analysis of satellite galaxy pairs (Ibata et al. 2014). Nevertheless, the cosmological challenge posted by the planes of satellite galaxies rests so far on only a small number of studied systems. For a better and statistically more reliable understanding, we need to aim for an as complete census of satellites around other nearby hosts as possible. Systems in the vicinity of the LG are accessible for follow-up measurements of photometric distances and line-of-sight velocities of its members. It allows one to understand their the three-dimensional structure and kinematics. Assembling a more complete picture of nearby satellite galaxy systems is thus fundamental to confirm some proposed formation scenarios for the observed alignments from an observational perspective, an urgently needed addition to complement the (so far) mostly simulation-driven debate.

Ultra-deep imaging in wide sky areas with amateur telescopes (Javanmardi et al. 2016; Romanowsky et al. 2016; Karachentsev et al. 2020) can also help to complete the census of these hitherto unknown low surface brightness (LSB) galaxies. In the last one and half decades, the discoveries of dwarf satellites in the LG have been made using stellar density maps of resolved stars, counted in selected areas of the color-magnitude diagrams (CMDs) from large scale surveys such as the Sloan Digital Sky Survey (SDSS) (e.g., Willman et al. 2005; Zucker et al. 2006), Pan-STARRs (e.g., Laevens et al. 2015), Dark Energy Survey (DES) (Dark Energy Survey Collaboration et al. 2016; Bechtol et al. 2015) and, more recently, the DECam Local Volume Exploration Survey (DELVE) (Drlica-Wagner et al. 2021; Mau et al. 2020), Hyper Suprime-Cam Subaru Strategic Program (HSC-SSP) (Homma et al. 2019) and the DESI Imaging Legacy surveys (Martinez-Delgado et al. 2021b).

In the case of the Milky Way, these diffuse systems are usually found as over-densities of old stellar populations in certain regions of the sky. Contamination by foreground stars and background galaxies makes this task challenging for diffuse sys-

tems. However, modern surveys are now routinely finding dwarf galaxies within the virial radius of the Milky Way (~ 300 kpc) (see the recent review by Simon 2019, and references therein). The larger distance of the Andromeda galaxy makes it prohibitive to resolve their stellar halo stars fainter than the red clump/horizontal branch level Dey et al. (e.g., PAndAS photometry: 2019). Thus, the M 31 satellite population can only be traced by observations of the less numerous, bright red-giant branch (RGB) stars. This means that the dwarf galaxy hunting in Andromeda is certainly biased due to the lack of enough stellar tracers for dwarf galaxies with absolute magnitude fainter than about -6 mag, which are barely resolved into stars with ground-based telescopes. In the last years, new generation large-scale imaging surveys (e.g., the DESI imaging Legacy surveys: Dey et al. 2019) have covered for the first time wide field regions around nearby galaxies at unprecedented low surface brightness regime (~ 28.0 – 28.5 mag arcsec $^{-2}$). This offers the possibility of detecting hitherto diffuse dwarf satellites by means of systematic searches based on visual inspection of these public images (e.g., Martinez-Delgado et al. 2021b) or on automatic detection algorithms (e.g., Greco et al. 2018; Tanoglidis et al. 2021; Müller & Schneider 2021; Prole et al. 2021; Haigh et al. 2021).

NGC 253 is one of the closest spirals behind M 31 and thus the natural place to dig for LSB dwarf galaxies that could provide new insights on the presence satellites planes around nearby galaxies outside the LG. At a distance of ~ 3.7 Mpc, this galaxy in the Sculptor group has been explored for satellite galaxies in the past (Cote et al. 1997; Karachentseva & Karachentsev 1998; Jerjen et al. 1998; Karachentseva & Karachentsev 2000; Jerjen et al. 2000; Sand et al. 2014; Toloba et al. 2016). In this paper, we present the discovery of three LSB dwarf galaxies near NGC 253 by a visual inspection of the DES imaging data. Using an updated census of low-mass systems around this galaxy, we address for the first time the issue of the existence of a spatially flattened and velocity-correlated dwarf galaxy system around NGC 253.

2. SEARCHING STRATEGY AND DATA ANALYSIS

2.1. Searching strategy

The dwarf galaxy candidates reported in this paper were found by the amateur astronomer Giuseppe Donatiello by visual inspection of the Dark Energy Camera (DECam: Flaugher et al. 2015) images of the Sculptor group of galaxies available from the DESI Legacy Imaging Surveys (Dey et al. 2019). A total number of 13 candidates were detected in an total explored area of 15×10 degrees. For this paper, we focus on only three candidates with clear evidence of being partially resolved into stars in the vicinity of NGC 253, as shown in Fig. 1 (left panel). The typical angular resolution of these data (estimated from the seeing of the images) is $\sim 0.9''$. We name them Donatiello II (Do II), Donatiello III (Do III) and Donatiello IV (Do IV), which position coordinates are given in Table 1. These galaxies have not been detected in the automatic search of diffuse stellar systems in the DES data undertaking by Tanoglidis et al. (2021).

2.2. Image cutout data

The DESI Legacy Imaging Surveys compile optical data in three optical bands (g , r and z) coupled with all-sky infrared imaging from the Wide-field Infrared Survey Explorer (WISE) (Wright et al. 2010; Meisner et al. 2019) and obtained by three different imaging projects on three different telescopes: The DECam Legacy Survey (DECaLS), the Beijing-Arizona Sky Sur-

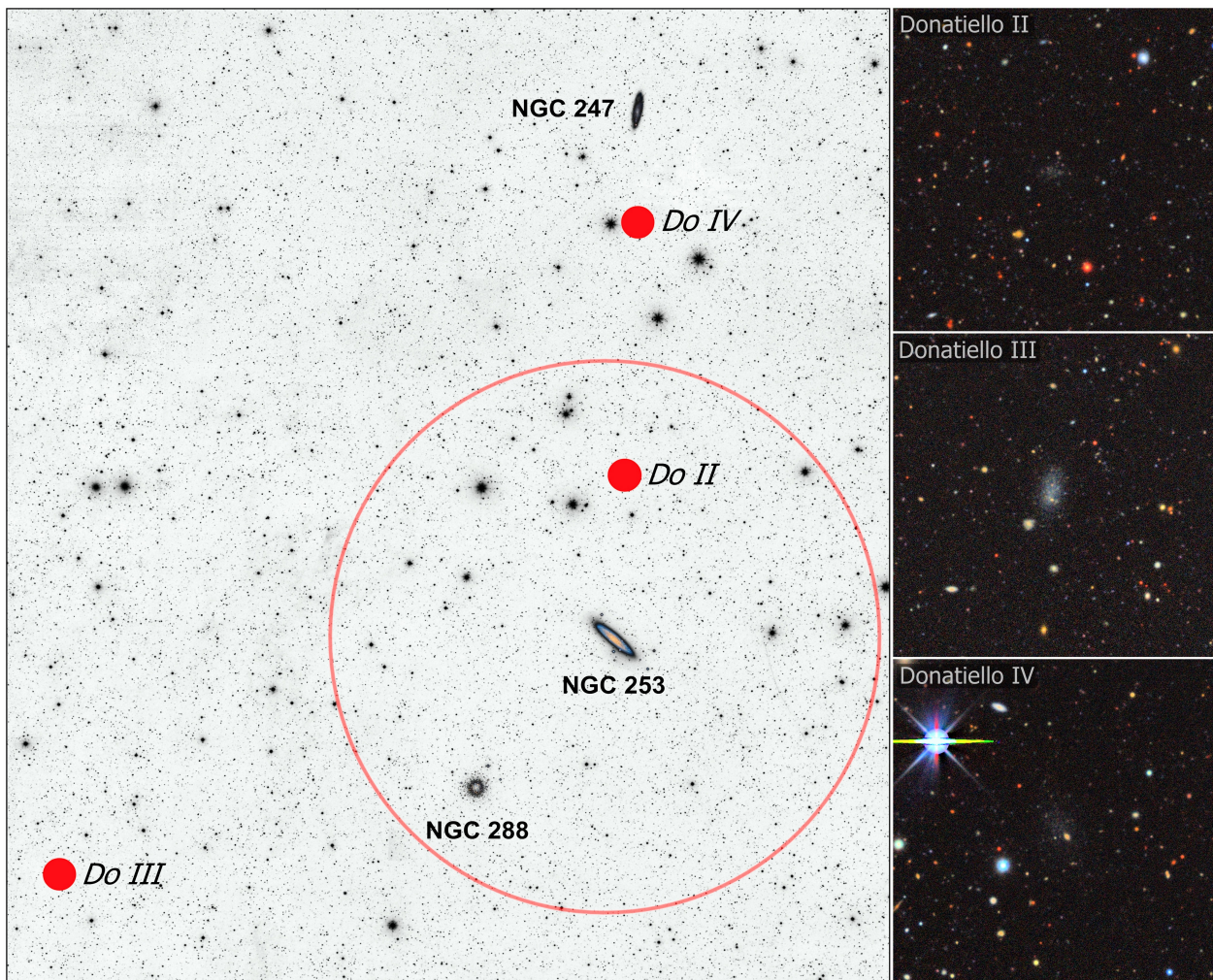


Fig. 1. (Left panel): The position of the three dwarf galaxies (solid red circles) reported in this study with respect to the spiral NGC 253. The red circular line corresponds to the area explored by the PISCes survey (Toloba et al. 2016) extending up to ~ 150 kpc from the center of NGC 253. The total field-of-view of this image is $450' \times 480'$. (Right panel): Full color version of the image cutouts obtained with *legacypipe* for Do II, Do III and Do IV. North is up and East is left. The field of view of all these image cutouts is $3.3' \times 3.3'$.

vey (BASS) and the Mayall z -band Legacy Survey (MzLS) (Zou et al. 2019; Dey et al. 2019). The DESI Legacy Imaging Surveys data releases also include re-reduced public DECam data from the DES (Abbott et al. 2018).

Image cutouts centered on each satellite candidate were subsequently obtained by coadding images of these systems taken by the DES (Dark Energy Survey Collaboration et al. 2016) using the DECam. These data were reprocessed using the *LEGACYPipe* software of the DESI Legacy imaging surveys (see, for example, Fig. 2 in Martínez-Delgado et al. 2021a). In short, each image is astrometrically calibrated to Gaia-DR2 and photometrically calibrated to the Pan-STARRS PS1 survey, and then resampled to a common pixel grid and summed with inverse-variance weighting. Fig. 1 (right panel) shows the resulting coadded image cutouts of the three dwarf galaxies, which include approximately 8 exposures in each of g , r , and z -bands. We have calculated the nominal depths of the images in the NGC 253 region following the approach by Román et al. (2020), appendix A. The calculated surface brightness limits are $\mu = 29.3$, 29.0 and 27.7 mag arcsec $^{-2}$ for the g , r and z bands respectively measured as 3σ in 10×10 arcsec boxes.

Table 1. The GALFIT results for the coordinate of the center of the galaxy, the Sersic index (n), Axis ratio (b/a), Position Angle (PA), and effective radius (R_{eff}). The V -band magnitude is estimated adopting the transformation equation provided by Jester et al. (2005). The physical parameters are calculated by adopting a distance modulus of 27.84 ± 0.02 mag (Jacobs et al. 2009) for NGC 253.

	Do II	Do III	Do IV
RA (J2000)	00 47 07.15	01 09 24.55	00 47 02.95
Dec (J2000)	-23 57 20.9	-27 20 49.6	-21 40 51.6
n	0.62 ± 0.12	0.56 ± 0.03	0.85 ± 0.12
b/a	0.61 ± 0.04	0.59 ± 0.01	0.60 ± 0.03
PA (deg)	-89.1 ± 5.2	-10.4 ± 1.6	$+24.0 \pm 3.7$
R_{eff} (arcsec)	5.51 ± 0.37	8.46 ± 0.17	10.21 ± 0.65
V (mag)	20.85 ± 0.20	18.75 ± 0.09	19.99 ± 0.15
M_V (mag)	-7.04 ± 0.20	-9.13 ± 0.09	-7.89 ± 0.15
R_{eff} (pc)	99 ± 7	152 ± 3	183 ± 12

2.3. Photometry and Structural Properties

We use GALFIT software (Peng et al. 2002) for determining the photometry and structural properties of dwarf galaxies following

a similar approach to that described in Javanmardi et al. (2016). First, the images of the three g , r , and z -bands are combined to increase the signal-to-noise and to perform the first GALFIT modelling. The center of the galaxy, Sersic index, axis ratio, position angle, and the effective radius are obtained from the combined images and the results are listed in Table 1. In the next step, to stabilize the fitting procedure, these parameters are kept fixed to their best values while fitting the individual band images for measuring the magnitude and surface brightness which are listed in Table 2. Fig. 2 shows the results of GALFIT modeling in r -band. The modeling for g and z -bands yields similar visual results hence are not shown here.

A careful inspection of the residual images (which is the result of subtracting the GALFIT model from the data) shows a number of unresolved sources which could belong to the dwarf galaxies. Among these unresolved sources, we mark those that pass the conditions $r > 24.0$ and $0.4 < g - r < 1.2$ by red circles.

Using the m_{Tot} values and adopting the transformation equation provided by Jester et al. (2005)¹ $V = g - 0.59 \times (g - r) - 0.01$, we obtain the V -band magnitudes. These results are also listed in Table 1. Table 2 shows as the surface brightness of these three stellar system is lower than 25 mag/arcsec^2) and thus cannot be detected in the previous photographic and CCD images from large-scale surveys like the POSS-II or PanSTARRs.

3. DISCUSSION

3.1. Distances

The DESI Legacy surveys images are not deep enough to build up a color-magnitude diagram of resolved stellar populations in these dwarf galaxies. Thus, it is not possible to determine their distance from the brightness of the tip of the RGB. Given their close angular distance to NGC 253, we assume that the discovered galaxies are at the same distance as NGC 253, following a similar approach to that used in other recent wide-field surveys of dwarf satellite systems in the local volume (Javanmardi et al. 2016; Carlsten et al. 2020). This is also supported by the degree of resolution into stars displayed for these new objects when it is compared with the images of some confirmed dwarf companions of NGC 253 obtained in the same survey (see Fig. 4). In addition, our hypothesis is consistent with the results from a standard approach used to establish membership based on the comparison of morphological and photometric properties with those from known dwarf galaxies (see for instance Müller et al. 2018a). In Table 1 we list the effective radius (in pc) and absolute magnitude, M_V (in mag), by assuming a distance modulus of $27.84 \pm 0.02 \text{ mag}$ (Jacobs et al. 2009) for NGC 253. Fig. 3 shows the distribution of these three dwarf galaxies in the R_e vs. L , μ_e vs. R_e , and μ_e vs. M_V planes. The known dwarf galaxies of the Milky Way and Andromeda (McConnachie 2012) are also shown for comparison. As can be seen, the three candidates can be characterized by similar properties as those of the LG dwarf galaxies, supporting our assumption that they could be located at a similar distance like that of NGC 253. However, with the present ground-based data, we cannot completely reject that some of these new dwarfs may be background galaxies projected onto the sky region of the Sculptor group.

3.2. The NGC 253 group of galaxies

Three new dwarf galaxies have been discovered in the vicinity of the bright late-type spiral NGC 253. This galaxy is the brightest member of the Sculptor filament (Jerjen et al. 1998; Karachentsev et al. 2003) located in the Local Supercluster plane almost in the Anti-Virgo direction. The distribution of galaxies over the sky in the Sculptor filament is shown in the Fig. 5. This region has been intensively studied in a number of H I surveys (see for instance Bouchard et al. 2005; Westmeier et al. 2017; Koribalski et al. 2018). The systematic searches of dwarf galaxies (Cote et al. 1997; Karachentseva & Karachentsev 1998; Jerjen et al. 1998; Karachentsev & Karachentsev 2000; Jerjen et al. 2000; Sand et al. 2014) have revealed a population of galaxies of very low luminosity down to $M_V \approx -10 \text{ mag}$. High-precision distances using the tip of the red giant branch (TRGB) were measured in the works by Karachentsev et al. (2003); Cannon et al. (2003); Mouhcine et al. (2005); Davidge (2006); Karachentsev et al. (2006); Mould & Sakai (2008); Jacobs et al. (2009); Dalcanton et al. (2009); Da Costa et al. (2009); Radburn-Smith et al. (2011); Lianou & Cole (2013); Sand et al. (2014); Toloba et al. (2016); Karachentsev et al. (2021).

The ‘tidal index’ (Karachentsev & Makarov 1999; Karachentsev et al. 2013) gives us a good proxy of group membership. It characterizes the degree of the tidal impact from the main disturber (MD) $TI \propto \log(L_{\text{MD}}/R_{\text{MD}}) + C$, where L_{MD} is a luminosity of the most influential neighbor and R_{MD} is its spatial separation from the galaxy under consideration. The constant C is chosen so that $TI = 0$ at the ‘zero-velocity surface’ of the main disturber. Thus, $TI > 0$ indicates that the galaxy is physically bound to its main disturber, while $TI < 0$ means that the object belongs to the field. We summarize information on galaxies in the vicinity of NGC 253 in the Table 3. Morphological type, absolute magnitude, ‘tidal index’ are given according to the current state of the Local Volume database² (Kaisina et al. 2012). Newly found galaxies are marked in bold. The hierarchy in the group is shown by intent in the galaxy name and the galaxies are sorted according to the ‘tidal index’ with respect to their main disturber. Data sources on velocities and distances are indicated as footnotes in the table. It is necessary to note that the velocity of NGC 253, $V_h = 261 \text{ km s}^{-1}$, obtained in the deep Parkes H I survey (Westmeier et al. 2017) differs significantly from other measurements. For instance, HIPASS Bright Galaxy Catalog (Koribalski et al. 2004) gives a systemic velocity $V_h = 243 \pm 2 \text{ km s}^{-1}$. Lucero et al. (2015) measure the velocity of the kinematical center of the galaxy of $V_h = 238 \pm 4 \text{ km s}^{-1}$ using H I radio-interferometric observations with the Karoo Array Telescope. However, to avoid possible systematic, we decided to use the value from the deep Parkes H I survey (Westmeier et al. 2017), because most velocity measurements around NGC 253 were taken from this survey. Note that the choice of one or another velocity of NGC 253 has practically no effect on the estimate of the total mass of the group.

Most galaxies in the Sculptor filament have precise TRGB distances. It allows us to map the 3D distribution of matter in this region. The projections of the spatial distribution of galaxies on the plane of the Local Supercluster and on the perpendicular plane are shown in the Fig. 6. At the moment there are 12 confirmed members in the group around NGC 253. Taking into account three new probable members and Sculptor SR for which there is no velocity or distance measurements the total

¹ <https://www.sdss.org/dr12/algorithms/sdssubvritransform>

² <https://www.sao.ru/lv/lvqdb/>

Table 2. First three rows: The GALFIT results for the integrated magnitude, m_G , the central surface brightness $\mu_{0,G}$ and the surface brightness at effective radius $\mu_{e,G}$ both in mag arcsec⁻² for g , r , and z -bands.

	Do II			Do III			Do IV		
	g	r	z	g	r	z	g	r	z
m_G	21.01 ± 0.15	20.75 ± 0.15	20.51 ± 0.15	19.13 ± 0.07	18.50 ± 0.05	18.26 ± 0.05	20.37 ± 0.12	19.74 ± 0.10	19.53 ± 0.12
$\mu_{0,G}$	25.66 ± 0.15	25.40 ± 0.15	25.16 ± 0.15	24.76 ± 0.07	24.13 ± 0.05	23.89 ± 0.05	25.97 ± 0.12	25.34 ± 0.10	25.13 ± 0.12
$\mu_{e,G}$	26.66 ± 0.15	26.40 ± 0.15	26.16 ± 0.15	25.64 ± 0.07	25.00 ± 0.05	24.77 ± 0.05	27.47 ± 0.12	26.84 ± 0.10	26.64 ± 0.12

Table 3. Galaxies in the vicinity of NGC 253. The columns contain: 1) galaxy name; 2) morphological type; 3) V_h – heliocentric velocity in km s⁻¹ with its error; 4) V_{LG} – radial velocity with respect to the LG centroid (Karachentsev & Makarov 1996); 5) D_{TRGB} – TRGB-distance in Mpc with a corresponding error; 6) M_B – B -band absolute magnitude of the galaxy; 7) TI – ‘tidal index’ indicating the value of the tidal influence from the main disturber (Karachentsev & Makarov 1999; Karachentsev et al. 2013); 8) Θ_{N253} – projected separation from NGC 253 in degrees; 9) R_{\perp} – projected distance to NGC 253 in kpc; 10) R_{3D} – spatial distance to NGC 253 in kpc.

Name	Type	V_h km s ⁻¹	V_{LG} km s ⁻¹	D_{TRGB} Mpc	M_B mag	TI	Θ_{N253} deg	R_{\perp} kpc	R_{3D} kpc
NGC 253	Sc	260.6 ± 5 ^a	294	3.70 ± 0.03 [†]	-21.15				
Do II	dSph				-6.6	3.2	1.3	86	
LV J0055–2310	dIr	249.6 ± 5 ^a	288	3.62 ± 0.18 [‡]	-9.81	2.2	2.7	175	191
Scl–MM–Dw1	dSph			3.94 ± 0.63 ^b	-9.54	1.8	1.1	71	251
NGC 247	Sd	153.0 ± 5 ^a	208	3.72 ± 0.03 [†]	-18.56	1.6	4.5	293	294
Do IV	dSph				-7.1	2.2	3.6	233	
ESO540–032	Ir	227.7 ± 0.9 ^b	285	3.63 ± 0.05 [†]	-11.45	1.4	5.4	349	354
Do III	dSph				-8.3	1.4	5.3	343	
DDO 6	dIr	295.3 ± 5 ^a	347	3.44 ± 0.15 [†]	-12.45	1.3	4.3	277	373
Sculptor SR	dTr				-10.26	1.2	4.0	257	
KDG 2	dTr	223.5 ± 2.7 ^b	290	3.56 ± 0.07 [†]	-11.49	1.0	7.2	463	478
Scl–MM–Dw2	dSph			3.12 ± 0.32 [#]	-11.03	0.7	0.8	53	582
Sc 22	dSph			4.29 ± 0.07 [†]	-10.50	0.5	5.4	350	699
NGC 7793	Sd	223.8 ± 5 ^a	247	3.63 ± 0.14 [†]	-18.34	0.2	13.1	842	838
PGC704814	Ir	270 ± 89 ^c	299	3.66 ± 0.18 [‡]	-11.61	2.1	12.4	798	795
ESO349–031	dIr	220.3 ± 5 ^a	229	3.21 ± 0.06 [†]	-11.87	0.2	12.6	802	901
DDO 226	dIr	362.1 ± 5 ^a	413	4.92 ± 0.29 [†]	-13.63	-0.3	3.2		1243
UGCA 442	Sm	266.7 ± 5 ^a	299	4.37 ± 0.15 [†]	-14.71	-0.3	15.5		1274
NGC 625	Sm	394.9 ± 5 ^a	324	4.02 ± 0.07 [†]	-16.50	-0.3	18.9		1307
NGC 59	dEem	367.6 ± 5 ^a	438	4.90 ± 0.07 [†]	-15.57	-0.4	8.3		1349
PGC 6430	Im	391.7 ± 5 ^a	306	4.57 ± 0.13 [†]	-15.68	-0.7	21.7		1778

^a Westmeier et al. (2017)[†] Jacobs et al. (2009)^b Sand et al. (2014)^b Bouchard et al. (2005)[‡] Karachentsev et al. (2021)[#] Toloba et al. (2016)^c Colless et al. (2003)

population consist of 16 galaxies. Only 9 of them have known radial velocities, that allows one to estimate the radial velocity dispersion in the NGC 253 group of 43 km s⁻¹. Most galaxies lie at a projection distance of less than 5.5° or about 350 kpc from NGC 253. In projection, Do II is the third nearest satellite of NGC 253. NGC 247 has high negative peculiar velocity of -86 km s⁻¹ with respect to NGC 253. In fact, Do IV together with ESO 540–032 form a subgroup around NGC 247. Do III, lying at a projected distance of about 340 kpc from NGC 253, is one of the peripheral members of the core of the group. Galaxies NGC 7793 with its companions PGC 704814 and ESO 349–031 are located near the border of the system. Obviously, these galaxies are just falling into the group center and, therefore, they cannot be used for the virial mass estimation. Other galaxies beyond 1 Mpc from NGC 253 participate in a general Hubble expansion, which allows Karachentsev et al. (2003) to determine the zero-velocity radius of the group to be 0.7 Mpc.

Starburst galaxy NGC 253 dominates the group. Its absolute magnitude is 2.6 mag less (in other words, 11 times brighter)

than the second brightest galaxy NGC 247. It allows us to use the virial theorem and the projected mass estimator in the simplest form of the test particles around a massive body (Bahcall & Tremaine 1981). Using the first five satellites of NGC 253 with known velocities (LV J0055–2310 + NGC 247 + ESO 540–032 + DDO 6 + KDG 2), we estimate the virial mass of the group to be $M_{vir} = 6.4 \times 10^{11} M_{\odot}$. The projected mass estimator, assuming isotropic orbits distribution $\langle e^2 \rangle = \frac{1}{2}$, gives a similar value of $M_{pm} = 7.1 \times 10^{11} M_{\odot}$. As we noticed before, these values are almost independent of the adopted velocity of NGC 253. In the case of a heliocentric radial velocity of $V_h = 243 \pm 2$ (Koribalski et al. 2004), the corresponding values are $M_{vir} = 6.2 \times 10^{11}$ and $M_{pm} = 6.8 \times 10^{11} M_{\odot}$. Taking into account that KDG 2 lying at a distance more than 460 kpc is most likely located outside the virial radius and excluding it from the analysis, for the 4 remaining satellites we obtain $M_{vir} = 7.3 \times 10^{11}$ and $M_{pm} = 8.8 \times 10^{11} M_{\odot}$. So, adopting the total mass of the NGC 253 group is about $8 \times 10^{11} M_{\odot}$, one can estimate the radius of the virialized region of $R_{200} = 186$ kpc, which corresponds to a sphere whose

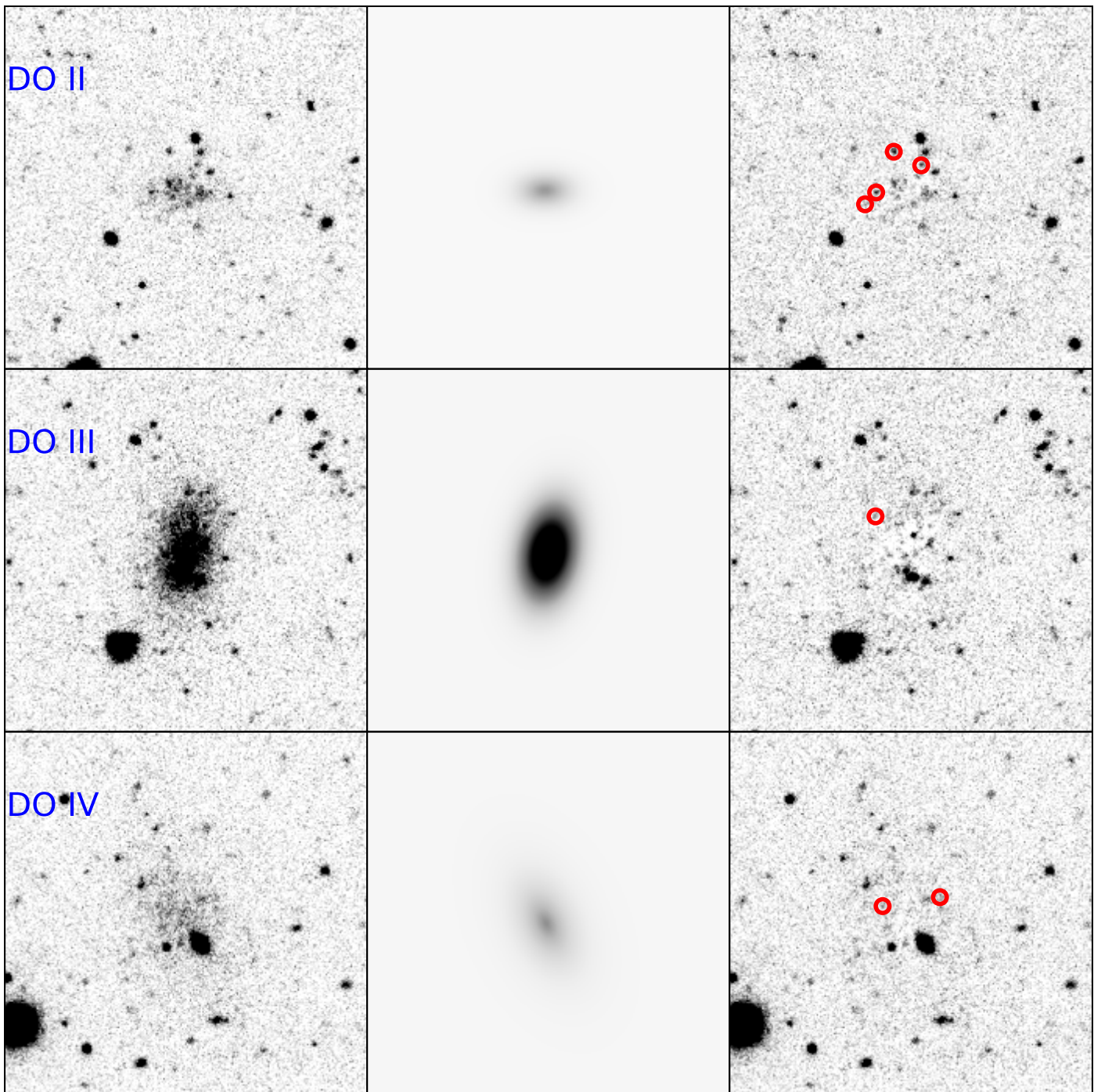


Fig. 2. From left to right: the dwarf galaxies in r -band, the GALFIT models, and the residual images after subtracting the model. The image scales and min max are the same for all the panels. The same procedure is done for modeling the g and z -band images. We mark the position of a few partially resolved resources in the galaxies that are visible in the residual images with red circles.

density is 200 times greater than the critical one. According to an exact analytical solution (Baushev 2019) the corresponding radius of the zero velocity surface is 706 kpc. This value is in excellent agreement with the direct measurement of the zero velocity radius of 0.7 Mpc by Karachentsev et al. (2003).

3.3. A Plane of Satellite Galaxies?

The presence of spatially flattened and velocity-correlated satellite galaxy systems around the Milky Way, M31, and Centau-

rus A motivates the question: Is there evidence for a similar alignment among the satellites of NGC 253?

Fig. 7 shows the on-sky distribution of the galaxies listed in Table 3, with the galaxies color-coded by their line-of-sight velocity component relative to the NGC 253 velocity. It is apparent from this figure that most of the known objects in the vicinity of NGC 253 align in an extremely narrow structure to the north. Of the 11 galaxies that potentially are within 600 kpc of NGC 253 (indicated by yellow boxes), only Do III and Sculptor SR are significantly offset from this orientation. Neither of these two have



Fig. 3. Comparison of the degree of resolution into stars of Do II in the DES images with the data from the same survey for two confirmed satellites of NGC 253 situated at similar distance (see Table 3): LVJ0055–2310 and Scl–MM–Dw1. The field-of-view of these image cutouts are $4' \times 4'$. North is up and East is left.

measured distances, so they could well be fore- or background objects outside of the system.

This asymmetric distribution of galaxies with respect to the NGC 253 can not be explained simply by the observational biases. The group is located near the South Galactic Pole, where the Galactic extinction is insignificant. A simple count of galaxies in a 30-degree cone around NGC 253 using the HyperLeda database (Makarov et al. 2014) shows that the redshift data is 97 per cent complete down to $B_T = 15.5$ and 86 per cent complete down to $B_T = 16.6$ mag. Thus we believe that we know velocities of all possible satellites in the group with $M_B \lesssim -12.3$ mag. Table 3 confirms this estimate. The only satellites without redshift measurements are dSph galaxies fainter than $M_B = -11$ mag. The hunt for more faint galaxies of extremely low surface brightness without gas is extremely difficult task, and our knowledge of the faint end of the galaxy luminosity function is highly incomplete below $M_B \sim -11$ mag. However, the brighter galaxies also show the similar spatial distribution, that appears to reflect the real structure of the group.

Of the eleven galaxies possibly within 600 kpc of NGC 253, eight are in the North and only three are in the South, and the asymmetry increases to six in the North and only one in the South if the four galaxies without distance measurements are excluded. The distribution of known galaxies around NGC 253 is thus strongly lopsided. While the asymmetry appears to be quite extreme in this case, lopsided distributions of galaxies around a host appear to be rather common: they have been found for the distribution of satellite galaxies around M31 (Conn et al. 2013), in statistical samples of both paired (Libeskind et al. 2016) and isolated galaxies (Brainerd & Samuels 2020), and even in cosmological simulations (Pawlowski et al. 2017; Wang et al. 2021).

It is intriguing that of the five galaxies with line-of-sight velocities, all of which align along the flattened structure to the North of NGC 253, four are blue- and only one is redshifted relative to NGC 253. This is well consistent with an interpretation as a mostly rotating satellite plane like those seen in M31 and Centaurus A. In fact, a fraction of 80 per cent correlated velocities is very similar to the fractions of correlated velocities reported for M31 (13 out of 15, or 86 per cent) by Ibata et al. (2013), and for Centaurus A (21 out of 28, or 75 per cent) by Müller et al. (2021a). However, due to the small number of objects, the degree of correlation for the NGC 253 system is not significant.

Finding a velocity coherence of at least 4 out of 5 happens in 37.5 per cent of all cases. A larger number of galaxies with measured velocities will thus be required for a statistically meaningful analysis, demonstrating an urgent need for spectroscopic follow-up of candidate dwarf galaxies in this region.

To study the three-dimensional distribution of the known satellites of NGC 253, we employ the common tensor-of-inertia (ToI) fitting method (see e.g. Pawlowski et al. 2015). We account for the uncertainties in the distance measurements by generating 1000 realizations of the observed system, drawing galaxy distances from normal distributions that are centered on their most-likely value and have a 1σ -width of the errors, as compiled in Table 3. We consider all galaxies within 600 kpc, excluding the four candidates without measured distances (Do II, III, IV and Sculptor SR). The results of our plane fits are compiled in Fig. 8. As expected from the flattened on-sky distribution, we find an extremely narrow spatial alignment: the root-mean-square (rms) height from the best-fit plane is only $\Delta_{\text{rms}} = 31 \pm 5$ kpc, and the minor-to-major axis ratio is $c/a = 0.14 \pm 0.03$. These values are comparable to those of the satellite planes around the Milky Way ($\Delta_{\text{rms}} = 20$ to 30 kpc, $c/a \approx 0.2$) and M31 ($\Delta_{\text{rms}} < 14.1$ kpc, $c/a \approx 0.1$). The normal direction to the best-fit plane is shown in Fig. 9. It points to Supergalactic Coordinates $(l_{\text{SG}}, b_{\text{SG}}) = (12^\circ, -73^\circ)$, and varies by only 4° around this direction. The plane has an inclination of $i = 85^\circ$, and is thus seen very close to edge-on – as is the case for the M31 and Centaurus A satellite structures. The good alignment with the Supergalactic plane could be related to the preference of flattened satellite galaxy structures in the Local Universe to align with the direction of greatest collapse of their surrounding larger-scale structure (Libeskind et al. 2019). This could also explain the preference to see these structures edge-on (since both the Milky Way and the nearby hosts lie in a common sheet-like structure). Indeed, as Fig. 9 shows the plane normal is closely aligned with the e_1 -direction, to within $(16.6 \pm 5.4)^\circ$, where e_1 is the eigenvectors of the tidal tensor at the position of NGC 253 which corresponds to the axis along which material in the cosmic web is compressed fastest. NGC 253 thus further confirms the finding in Libeskind et al. (2018) that some flattened dwarf galaxy structures in the Local Universe preferentially align with the e_1 -direction at their respective positions, and thus appear to be related to the larger-scale cosmic web.

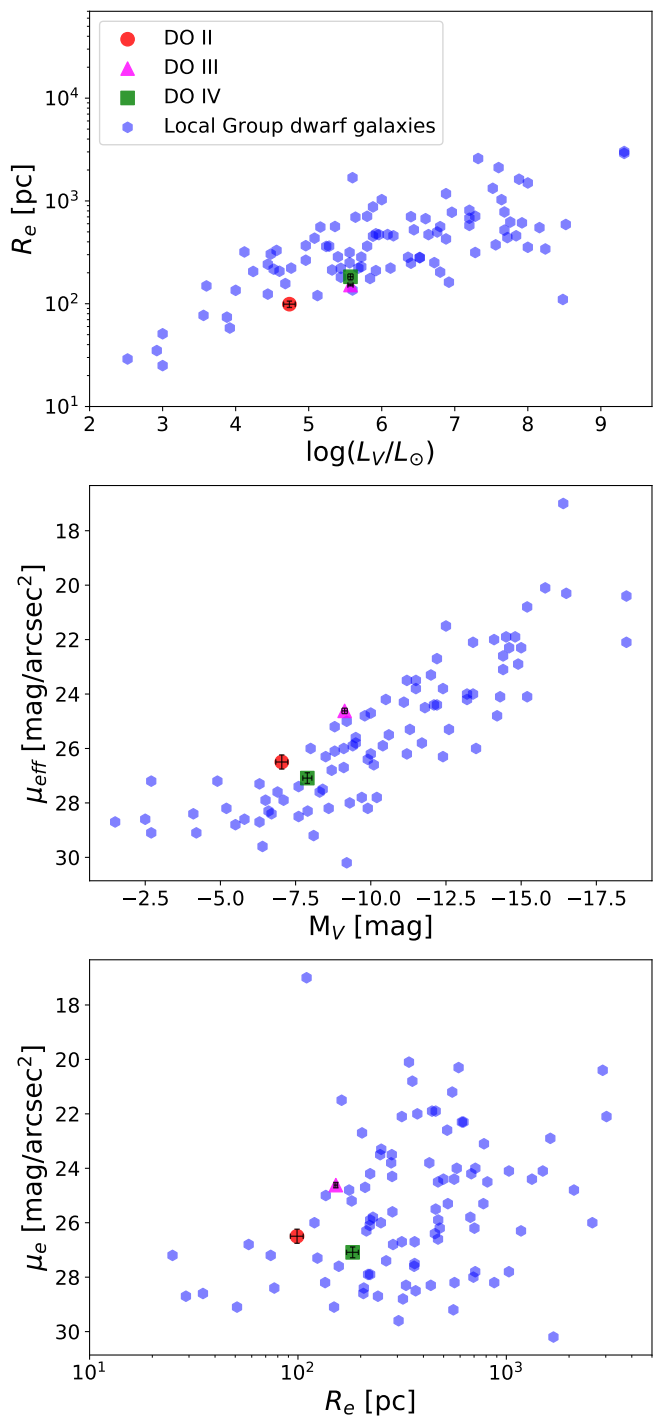


Fig. 4. Comparison of the photometric and structural parameters of the three dwarf galaxies reported in this study with those for the Milky Way and M 31 companions.

To assess the significance of the found flattening compared to completely random, uncorrelated distributions, we repeat the plane-fitting on randomized systems. These are drawn from an isotropic distribution centered on NGC 253, but follow the exact same radial distances from the host as our observed realizations (grey histograms in the figure). The isotropic distributions typically results in much wider plane fits, and the flattening measured for the observed system are off by 2σ for both the absolute plane height and the relative axis ratios. Thus, while not highly

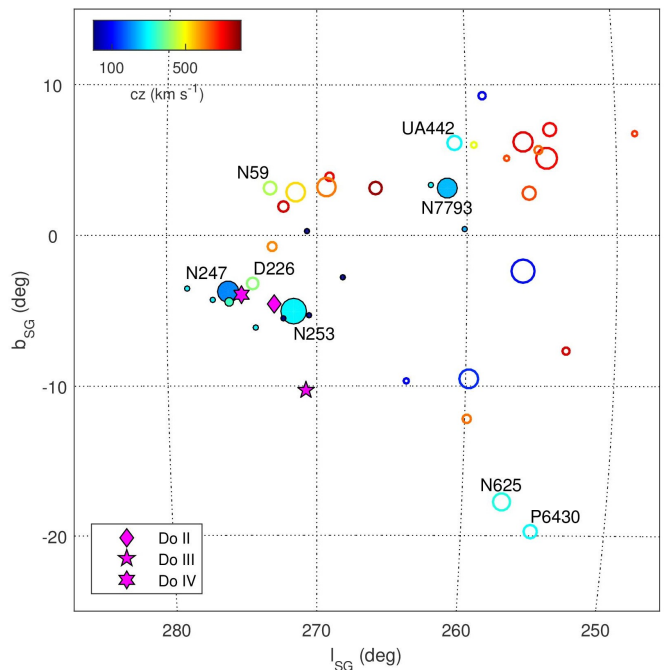


Fig. 5. Distribution of galaxies around NGC 253 in a $40^\circ \times 40^\circ$ field in the supergalactic coordinates. The members of the NGC 253 group are shown by filled colored circles. The background (reddish) and foreground (bluish) galaxies are marked with open circles. The redshift is color-coded accordingly the color schema. Newly discovered objects are shown by magenta polygons.

significant – as expected given the small number of objects – it is still an intriguing alignment that warrants further study of this system’s phase-space correlation, in particular via distance measurements of other satellite galaxy candidates to assess their association with NGC 253.

While a detailed comparison to cosmological expectations is beyond the scope of the present work, we nevertheless illustrate the expected flattening of satellite galaxy systems in Λ CDM by comparing to systems in the Illustris TNG-100 hydrodynamical cosmological simulation (Springel et al. 2018; Nelson et al. 2019). As analogs, we select host galaxies with virial masses in the range of 0.6 to $1.0 \times 10^{12} M_\odot$, which are required to be sufficiently isolated by rejecting all hosts that have another galaxy with a virial mass exceeding $0.5 \times 10^{12} M_\odot$ within 1.2 Mpc. The galaxies within a volume of 600 kpc around each host are ranked based on their brightness (if they contain stars), followed by a ranking by mass (if they are dark). The flattening of the seven top-ranked galaxies (excluding the host) is measured, and the resulting distribution of absolute plane height, relative axis ratio, and best-fit plane’s offset from the host are plotted in red in Fig. 8.

As expected, the Λ CDM satellite systems are more flattened than systems drawn from isotropy (especially because the considered volume exceeds the virial volume of the simulated hosts). However, the observed distribution of galaxies around NGC 253 remains on the more flattened tail of the distribution: only $10.1^{+7.2}_{-5.3}$ and $12.5^{+6.8}_{-4.6}$ per cent of the simulated systems are more flattened than the observed system in c/a and Δ_{rms} , respectively (where the error bars are based on the standard deviations obtained from the Monte-Carlo sampling of the observed distribution). The flattened distribution of the presently confirmed galaxies in the vicinity of NGC 253 thus does not rise to the same

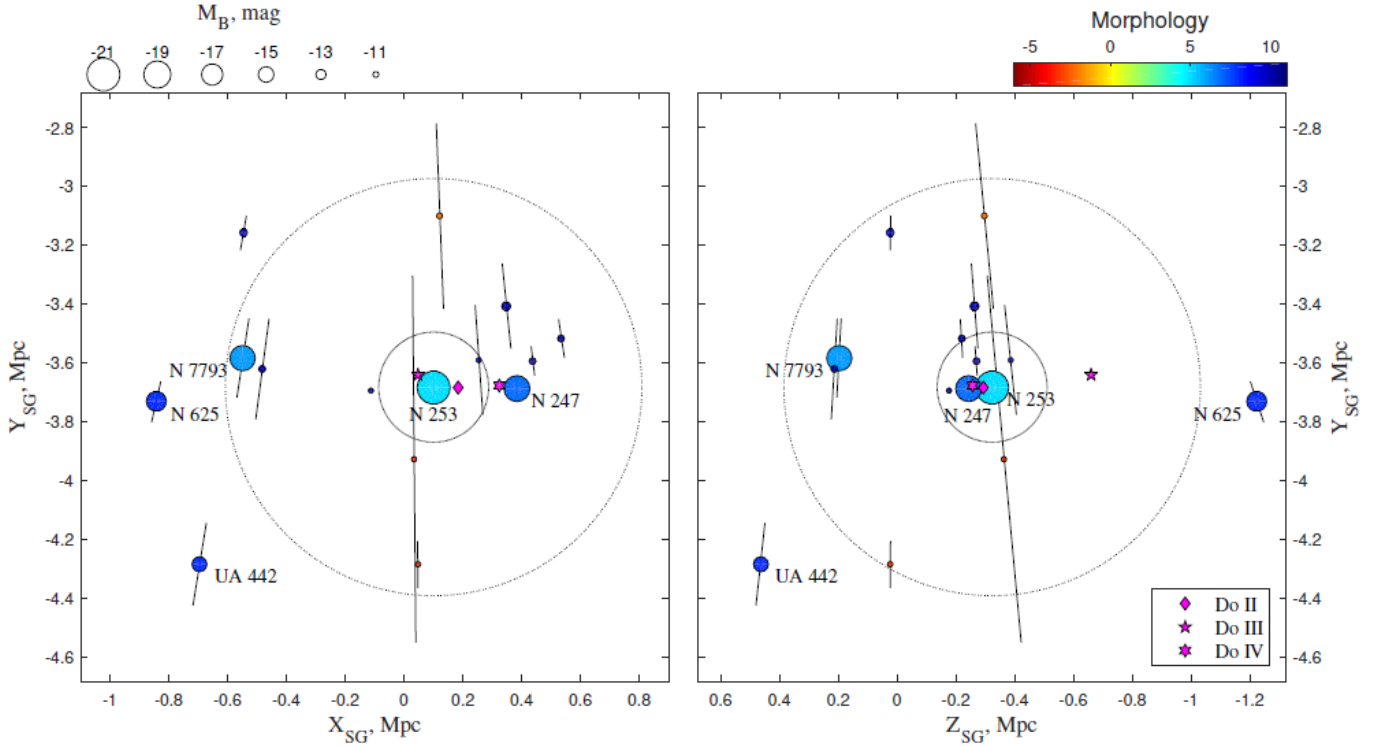


Fig. 6. The map of galaxies in the vicinity of NGC 253 in the supergalactic coordinates. The left-hand panel presents the XY-projection on the supergalactic plane, while the right-hand panel shows the edge-on view of the Local Supercluster ‘pancake’. The size and color of the dots correspond to the absolute B -band magnitude and morphology of galaxies, according to the schemes. The line segments indicate uncertainties in the distance estimations. Big circles around NGC 253 mark the virial zone, $R_{200} \approx 190$ kpc, and the zero velocity surface, $R_0 \approx 700$ kpc. The magenta symbols indicate the expected position of the discovered galaxies.

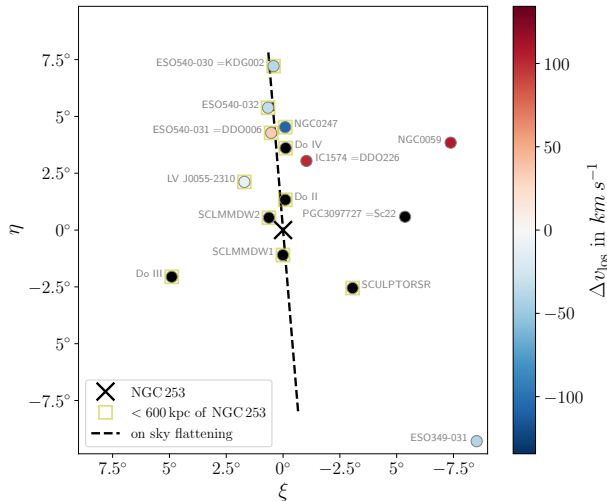


Fig. 7. On-sky distribution of the galaxies listed in Table 3 in equatorial coordinates relative to the position of NGC 253 (black cross). The galaxies are color-coded by their line-of-sight velocity component relative to the NGC 253 velocity. Galaxies without velocity measurements are plotted in black. Galaxies (potentially) within 600 kpc of NGC 253 are marked with yellow boxes. The dashed black line indicates the on-sky orientation of the flattening of these objects.

degree of tension reported for the better-studied satellite galaxy planes around the Milky Way, M31, and Centaurus A.

If, however, only one additional satellite would be confirmed, without changing the overall measured flattening of the system, then the fractions reported above would already drop by about a factor of two, to $5.4^{+4.9}_{-2.9}$ and $7.1^{+5.0}_{-3.6}$ per cent of simulated systems being more flattened in c/a and Δ_{rms} , respectively. This demonstrated that it will require a more complete census of galaxies around NGC 253 via distance measurements of the current candidates, as well as a more complete sample of spectroscopic velocity measurements, to clarify whether the system is indeed exceptional, or rather typical, compared to expectations derived from cosmological simulations.

If we assume that the galaxies (including our new three discoveries) for which no distance measurement exist are at the distance of NGC 253, with a broad distance uncertainty of ± 200 kpc, our plane fits become less extreme. The broad assumed distance uncertainties also introduce a lot of scatter in the obtained best-fit parameters. While the best-fit orientation changes only mildly, the plane width are then dominated by the two spatial outliers Do III and Sculptor SR.

While one can interpret the spatial alignment as a potential plane of satellite galaxies, its extent of 600 kpc exceeds the virial volume of NGC 253. This makes the structure more similar to the larger-scale planes of dwarf galaxies discovered in the LG, which have diameters of 1–2 Mpc (Pawlowski et al. 2013). However, even the 6 galaxies (assuming those without distance measurements share the same distance as NGC 253) within 300 kpc are roughly aligned in the same direction as the objects on larger

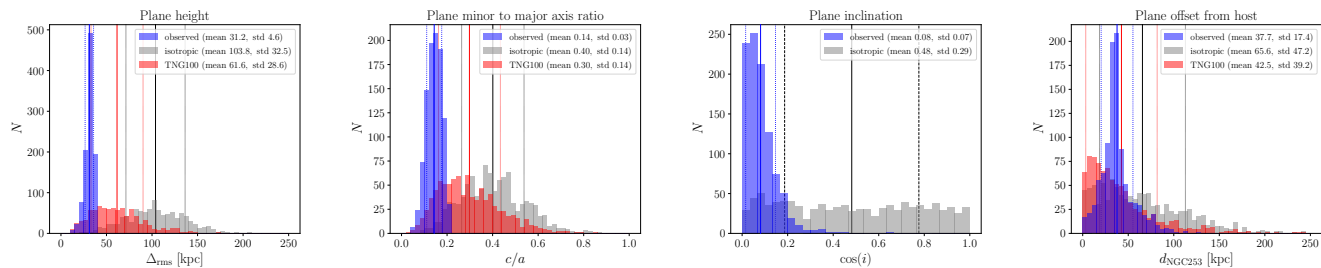


Fig. 8. Best-fit parameters for the ToI fits to the spatial distributions of galaxies within 600 kpc of NGC 253. Shown are, from left to right: the absolute rms plane height Δ_{rms} , the relative minor-to-major axis ratio c/a , the inclination i of the best-fit plane with the line-of-sight to NGC 253, and the perpendicular offset $d_{\text{NGC}253}$ of the best-fit plane from the host galaxy NGC 253 (which was not included in the plane fit). Each panel also gives the mean and standard deviations of the shown distributions. The realizations drawing from the observed galaxy distances (blue) are much more flattened (by both measures) than the randomized samples (grey) drawn from isotropic distributions around NGC 253’s position but following the same radial distances. Satellite systems drawn from the Illustris TNG 100 simulation (red) are more flattened than isotropic distributions in both absolute plane height and axis ratio, but the observed system falls onto the more flattened tail of their distribution.

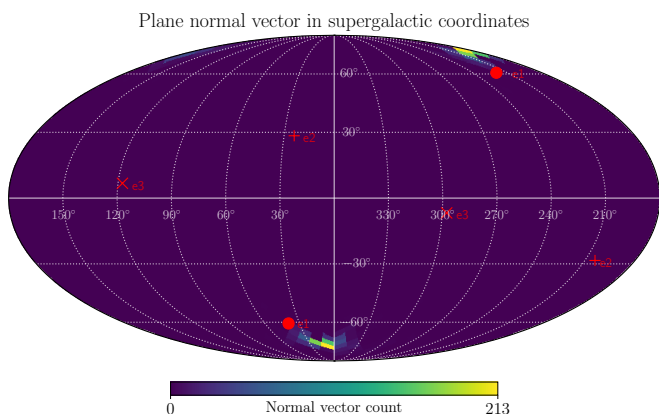


Fig. 9. Density distribution of the direction of plane-normal vectors (minor axis of 3D galaxy distribution) of the galaxies with measured distances within 600 kpc around NGC 253, for 1000 realizations drawing from the distance errors. Shown are Supergalactic Coordinates, indicating that the best-fit plane aligns closely with the Supergalactic Plane. The red symbols indicate the eigenvectors of the tidal tensor at the position of NGC 253, which describe the principal directions of the surrounding cosmic web. The best-fit plane is well aligned with e_1 , the axis along which material in the cosmic web is compressed fastest.

scales. Another interpretation of the larger structure is that these galaxies trace a cosmic filament. Preferential accretion of dwarf galaxies along filaments was proposed as a possible origin of flattened satellite galaxy structures (Lovell et al. 2011; Libeskind et al. 2011). While the alignment of the flattened galaxy distribution with the direction of fastest collapse of the surrounding cosmic web can be seen as support of such an interpretation, the observed distribution appears much more narrow than a typical filament in cosmological simulations, and the resulting satellite galaxy systems in simulations are typically not highly anisotropic (Pawlowski et al. 2012; Shao et al. 2018). However, since the effects of accretion along filament on the formation of satellite alignments have thus far mostly been studied in cosmological simulations, NGC 253 promises to be a unique observational test case of the filamentary accretion scenario: a potential satellite plane in the making by the cosmic web.

4. Conclusions

In this study we report the discovery of three dwarf spheroidal galaxies, named Do II, Do III and Do IV, in the vicinity of the bright late-type spiral NGC 253 galaxy by means of a visual inspection of the images taken by the DES. For our analysis, the images were processed using the LEGACYPIPE software from the DESI Legacy imaging surveys. We used the GALFIT software for deriving their photometric and structural properties. The physical parameters for Do II, Do III and Do IV were calculated by adopting a distance modulus of 27.84 ± 0.02 mag for NGC 253 (Jacobs et al. 2009). The resulting total absolute magnitudes of the dwarfs transformed to the V -band fall in the range from about -7 to about -9 mag, which are typical for satellite dwarf galaxies in the Local Universe. The central surface brightness tend to be extremely low for all the discovered dwarfs and fall roughly in the range of 25 – 26 mag arcsec $^{-2}$ in g -band.

So far there are 12 confirmed members in the group around NGC 253. Taking into account these three possible new members and the Sculptor SR dwarf galaxy, the total population consists of 16 galaxies. The radial velocity dispersion in the NGC 253 group estimated using the nine members with known radial velocities is 43 km s $^{-1}$. Most galaxies lie at a projected distance of less than 5.5° or about 350 kpc from NGC 253. Do II is the third nearest in projection satellite of NGC 253. The late spiral galaxy NGC 247 has high negative peculiar velocity of -86 km s $^{-1}$ with respect to NGC 253. In fact, Do IV together with the dwarf irregular galaxy ESO 540–032 forms a subgroup around NGC 247. Do III, lying at a distance of about 340 kpc from NGC 253, is one of the peripheral members of the core of the group.

We have used the virial theorem and the projected mass estimator to determine the galaxy group mass. We estimated the total mass of the NGC 253 group to be about $8 \times 10^{11} M_\odot$. Therefore, the respective estimated radius of the virialized region is $R_{200} = 186$ kpc, and the corresponding radius of the zero velocity surface is 706 kpc.

We also discuss the issue of the possible existence of a spatially flattened and velocity-correlated satellite galaxy system around NGC 253. It is apparent from our analysis that most of the known objects in the vicinity of NGC 253 are aligned in an extremely narrow structure to the North side of the galaxy. Of the 12 galaxies that potentially are within 600 kpc from NGC 253, only Do III and Sculptor SR are significantly offset from this orientation.

To study the three-dimensional distribution of the known satellites of NGC 253, we have employed the common tensor-

of-inertia fitting method. As expected from a flattened on-sky distribution, we have found an extremely narrow spatial alignment: the root-mean-square (rms) height from the best-fit plane is only $\Delta_{\text{rms}} = 31 \pm 5$ kpc, and the minor-to-major axis ratio is $c/a = 0.14 \pm 0.03$. These values are comparable to those of the satellite planes found around the Milky Way and M31. While one can interpret this alignment as a potential plane of satellite galaxies, its extension of 600 kpc exceeds the virial volume of NGC 253. This makes the structure more similar to the larger-scale planes of dwarf galaxies discovered in the LG, which have diameters of 1–2 Mpc (Pawlowski et al. 2013).

The first results of our survey of dwarf galaxies around NGC 253 or the recent discovery of a possible very faint satellite of M33 (Martínez-Delgado et al. 2021b) demonstrated the suitability of DESI Legacy surveys imaging for discovering diffuse satellites of nearby spiral galaxies by means of the visual inspection of the images. Because of the low surface brightness of the three dwarf galaxies reported here, their association with NGC 253 can be only confirmed with TRGB estimates in CMDs from deeper HST data and ground-based 8-meter telescopes or, alternatively, radial velocities obtained with state-of-the-art spectroscopic instruments (e.g., Müller et al. 2021b).

Acknowledgements. We thank the referee for giving constructive comments which substantially helped improving this paper. We also thank Noam Libeskind, Martha Haynes and Lister Staveley-Smith for useful comments. DMD acknowledges financial support from the Talentia Senior Program (through the incentive ASE-136) from Secretaría General de Universidades, Investigación y Tecnología, de la Junta de Andalucía. DMD also acknowledges funding from the State Agency for Research of the Spanish MCIU through the “Center of Excellence Severo Ochoa” award to the Instituto de Astrofísica de Andalucía (SEV-2017-0709). MSP thanks the Klaus Tschira Stiftung and German Scholars Organization for support via a KT Boost Fund. JR acknowledge financial support from the grants AYA2015-65973-C3-1-R and RTI2018-096228-B-C31 (MINECO/FEDER, UE) as well as support from the State Research Agency (AEI-MCINN) of the Spanish Ministry of Science and Innovation under the grant “The structure and evolution of galaxies and their central regions” with reference PID2019-105602GB-I00/10.13039/501100011033. We acknowledge the usage of the HyperLeda database³ (Makarov et al. 2014). This project used public archival data from the Dark Energy Survey. Funding for the DES Projects has been provided by the U.S. Department of Energy, the U.S. National Science Foundation, the Ministry of Science and Education of Spain, the Science and Technology Facilities Council of the United Kingdom, the Higher Education Funding Council for England, the National Center for Supercomputing Applications at the University of Illinois at Urbana-Champaign, the Kavli Institute of Cosmological Physics at the University of Chicago, the Center for Cosmology and Astro-Particle Physics at the Ohio State University, the Mitchell Institute for Fundamental Physics and Astronomy at Texas A&M University, Financiadora de Estudos e Projetos, Fundação Carlos Chagas Filho de Amparo à Pesquisa do Estado do Rio de Janeiro, Conselho Nacional de Desenvolvimento Científico e Tecnológico and the Ministério da Ciência, Tecnologia e Inovação, the Deutsche Forschungsgemeinschaft, and the Collaborating Institutions in the Dark Energy Survey. The Collaborating Institutions are Argonne National Laboratory, the University of California at Santa Cruz, the University of Cambridge, Centro de Investigaciones Energéticas, Medioambientales y Tecnológicas-Madrid, the University of Chicago, University College London, the DES-Brazil Consortium, the University of Edinburgh, the Eidgenössische Technische Hochschule (ETH) Zürich, Fermi National Accelerator Laboratory, the University of Illinois at Urbana-Champaign, the Institut de Ciències de l’Espai (IEEC/CSIC), the Institut de Física d’Altes Energies, Lawrence Berkeley National Laboratory, the Ludwig-Maximilians Universität München and the associated Excellence Cluster Universe, the University of Michigan, the National Optical Astronomy Observatory, the University of Nottingham, The Ohio State University, the OzDES Membership Consortium, the University of Pennsylvania, the University of Portsmouth, SLAC National Accelerator Laboratory, Stanford University, the University of Sussex, and Texas A&M University. Based in part on observations at Cerro Tololo Inter-American Observatory, National Optical Astronomy Observatory, which is operated by the Association of Universities for Research in Astronomy (AURA) under a cooperative agreement with the National Science Foundation.

References

- Abbott, T. M. C., Abdalla, F. B., Allam, S., et al. 2018, *ApJS*, 239, 18
 Bahcall, J. N. & Tremaine, S. 1981, *ApJ*, 244, 805
 Baushev, A. N. 2019, *MNRAS*, 490, L38
 Bechtol, K., Drlica-Wagner, A., Balbinot, E., et al. 2015, *ApJ*, 807, 50
 Bennet, P., Sand, D. J., Crnojević, D., et al. 2019, arXiv e-prints, arXiv:1906.03230
 Bouchard, A., Jerjen, H., Da Costa, G. S., & Ott, J. 2005, *AJ*, 130, 2058
 Brainerd, T. G. & Samuels, A. 2020, *ApJ*, 898, L15
 Bullock, J. S. & Boylan-Kolchin, M. 2017, *ARA&A*, 55, 343
 Cannon, J. M., Dohm-Palmer, R. C., Skillman, E. D., et al. 2003, *AJ*, 126, 2806
 Carlsten, S. G., Greco, J. P., Beaton, R. L., & Greene, J. E. 2020, *ApJ*, 891, 144
 Chiboucas, K., Jacobs, B. A., Tully, R. B., & Karachentsev, I. D. 2013, *The Astronomical Journal*, 146, 126
 Colless, M., Peterson, B. A., Jackson, C., et al. 2003, arXiv e-prints, astro
 Conn. A. R., Lewis, G. F., Ibata, R. A., et al. 2013, *ApJ*, 766, 120
 Cote, S., Freeman, K. C., Carignan, C., & Quinn, P. J. 1997, *AJ*, 114, 1313
 Da Costa, G. S., Grebel, E. K., Jerjen, H., Rejkuba, M., & Sharina, M. E. 2009, *AJ*, 137, 4361
 Dalcanton, J. J., Williams, B. F., Seth, A. C., et al. 2009, *ApJS*, 183, 67
 Dark Energy Survey Collaboration, Abbott, T., Abdalla, F. B., et al. 2016, *MNRAS*, 460, 1270
 Davidge, T. J. 2006, *ApJ*, 641, 822
 Dey, A., Schlegel, D. J., Lang, D., et al. 2019, *AJ*, 157, 168
 Drlica-Wagner, A., Carlin, J. L., Nidever, D. L., et al. 2021, arXiv e-prints, arXiv:2103.07476
 Flaugh, B., Diehl, H. T., Honscheid, K., et al. 2015, *AJ*, 150, 150
 Fritz, T. K., Battaglia, G., Pawlowski, M. S., et al. 2018, *A&A*, 619, A103
 Grebel, E. K. 2005, in *American Institute of Physics Conference Series*, Vol. 752, *Stellar Astrophysics with the World’s Largest Telescopes*, ed. J. Mikolajewska & A. Olech, 161–174
 Greco, J. P., Greene, J. E., Strauss, M. A., et al. 2018, *ApJ*, 857, 104
 Haigh, C., Chamba, N., Venhola, A., et al. 2021, *A&A*, 645, A107
 Homma, D., Chiba, M., Komiyama, Y., et al. 2019, *PAJ*, 71, 94
 Ibata, R. A., Ibata, N. G., Lewis, G. F., et al. 2014, *ApJ*, 784, L6
 Ibata, R. A., Lewis, G. F., Conn, A. R., et al. 2013, *Nature*, 493, 62
 Jacobs, B. A., Rizzi, L., Tully, R. B., et al. 2009, *AJ*, 138, 332
 Javanmardi, B. & Kroupa, P. 2020, *MNRAS*, 493, L44
 Javanmardi, B., Martínez-Delgado, D., Kroupa, P., et al. 2016, *A&A*, 588, A89
 Jerjen, H., Binggeli, B., & Freeman, K. C. 2000, *AJ*, 119, 593
 Jerjen, H., Freeman, K. C., & Binggeli, B. 1998, *AJ*, 116, 2873
 Jester, S., Schneider, D. P., Richards, G. T., et al. 2005, *AJ*, 130, 873
 Kaisina, E. I., Makarov, D. I., Karachentsev, I. D., & Kaisin, S. S. 2012, *Astrophysical Bulletin*, 67, 115
 Karachentsev, I. D., Dolphin, A., Tully, R. B., et al. 2006, *AJ*, 131, 1361
 Karachentsev, I. D., Grebel, E. K., Sharina, M. E., et al. 2003, *A&A*, 404, 93
 Karachentsev, I. D. & Makarov, D. A. 1996, *AJ*, 111, 794
 Karachentsev, I. D. & Makarov, D. I. 1999, in *Galaxy Interactions at Low and High Redshift*, ed. J. E. Barnes & D. B. Sanders, Vol. 186, 109
 Karachentsev, I. D., Makarov, D. I., & Kaisina, E. I. 2013, *AJ*, 145, 101
 Karachentsev, I. D., Neyer, F., Späni, R., & Zilch, T. 2020, *Astronomische Nachrichten*, 341, 1037
 Karachentsev, I. D., Tully, R. B., Anand, G. S., Rizzi, L., & Shaya, E. J. 2021, arXiv e-prints, arXiv:2102.11354
 Karachentseva, V. E. & Karachentsev, I. D. 1998, *A&AS*, 127, 409
 Karachentseva, V. E. & Karachentsev, I. D. 2000, *A&AS*, 146, 359
 Koribalski, B. S., Staveley-Smith, L., Kilborn, V. A., et al. 2004, *AJ*, 128, 16
 Koribalski, B. S., Wang, J., Kamphuis, P., et al. 2018, *MNRAS*, 478, 1611
 Kroupa, P., Haghi, H., Javanmardi, B., et al. 2018, *Nature*, 561, E4
 Laevens, B. P. M., Martin, N. F., Bernard, E. J., et al. 2015, *ApJ*, 813, 44
 Li, H., Hammer, F., Babusiaux, C., et al. 2021, arXiv e-prints, arXiv:2104.03974
 Lianou, S. & Cole, A. A. 2013, *A&A*, 549, A47
 Libeskind, N. I., Carlesi, E., Müller, O., et al. 2019, *MNRAS*, 490, 3786
 Libeskind, N. I., Guo, Q., Tempel, E., & Ibata, R. 2016, *ApJ*, 830, 121
 Libeskind, N. I., Knebe, A., Hoffman, Y., et al. 2011, *MNRAS*, 411, 1525
 Libeskind, N. I., van de Weygaert, R., Cautun, M., et al. 2018, *MNRAS*, 473, 1195
 Lovell, M. R., Eke, V. R., Frenk, C. S., & Jenkins, A. 2011, *MNRAS*, 413, 3013
 Lucero, D. M., Carignan, C., Elson, E. C., et al. 2015, *MNRAS*, 450, 3935
 Makarov, D., Prugniel, P., Terekhova, N., Courtois, H., & Vauglin, I. 2014, *A&A*, 570, A13
 Martínez-Delgado, D., Cooper, A. P., Roman, J., et al. 2021a, arXiv e-prints, arXiv:2104.06071
 Martínez-Delgado, D., Karim, N., Boschin, W., et al. 2021b, arXiv e-prints, arXiv:2104.03859
 Mau, S., Cerny, W., Pace, A. B., et al. 2020, *ApJ*, 890, 136
 McConnachie, A. W. 2012, *AJ*, 144, 4
 Meisner, A. M., Lang, D., Schlafly, E. F., & Schlegel, D. J. 2019, *PASP*, 131, 124504

³ <http://leda.univ-lyon1.fr>

- Mouhcine, M., Ferguson, H. C., Rich, R. M., Brown, T. M., & Smith, T. E. 2005, *ApJ*, 633, 810
- Mould, J. & Sakai, S. 2008, *ApJ*, 686, L75
- Müller, O., Jerjen, H., & Binggeli, B. 2018a, *A&A*, 615, A105
- Müller, O., Pawłowski, M. S., Jerjen, H., & Lelli, F. 2018b, *Science*, 359, 534
- Müller, O., Pawłowski, M. S., Lelli, F., et al. 2021a, *A&A*, 645, L5
- Müller, O., Pawłowski, M. S., Lelli, F., et al. 2021b, *A&A*, 645, L5
- Müller, O. & Schneider, E. 2021, *The Open Journal of Astrophysics*, 4, 3
- Nelson, D., Springel, V., Pillepich, A., et al. 2019, *Computational Astrophysics and Cosmology*, 6, 2
- Pawłowski, M. S. 2018, *Modern Physics Letters A*, 33, 1830004
- Pawłowski, M. S., Famaey, B., Merritt, D., & Kroupa, P. 2015, *ApJ*, 815, 19
- Pawłowski, M. S., Ibata, R. A., & Bullock, J. S. 2017, *ApJ*, 850, 132
- Pawłowski, M. S. & Kroupa, P. 2013, *MNRAS*, 435, 2116
- Pawłowski, M. S., Kroupa, P., Angus, G., et al. 2012, *MNRAS*, 424, 80
- Pawłowski, M. S., Kroupa, P., & Jerjen, H. 2013, *MNRAS*, 435, 1928
- Peng, C. Y., Ho, L. C., Impey, C. D., & Rix, H.-W. 2002, *AJ*, 124, 266
- Prole, D. J., van der Burg, R. F. J., Hilker, M., & Spitler, L. R. 2021, *MNRAS*, 500, 2049
- Radburn-Smith, D. J., de Jong, R. S., Seth, A. C., et al. 2011, *ApJS*, 195, 18
- Román, J., Trujillo, I., & Montes, M. 2020, *A&A*, 644, A42
- Romanowsky, A. J., Martínez-Delgado, D., Martín, N. F., et al. 2016, *MNRAS*, 457, L103
- Sand, D. J., Crnojević, D., Strader, J., et al. 2014, *ApJ*, 793, L7
- Shao, S., Cautun, M., Frenk, C. S., et al. 2018, *MNRAS*, 476, 1796
- Simon, J. D. 2019, *ARA&A*, 57, 375
- Smercina, A., Bell, E. F., Price, P. A., et al. 2018, *ApJ*, 863, 152
- Sohn, S. T., Patel, E., Fardal, M. A., et al. 2020, *ApJ*, 901, 43
- Springel, V., Pakmor, R., Pillepich, A., et al. 2018, *MNRAS*, 475, 676
- Tanoglidis, D., Drlica-Wagner, A., Wei, K., et al. 2021, *ApJS*, 252, 18
- Toloba, E., Sand, D. J., Spekkens, K., et al. 2016, *ApJ*, 816, L5
- Tolstoy, E. 2000, *arXiv e-prints*, astro
- Tully, R. B., Libeskind, N. I., Karachentsev, I. D., et al. 2015, *ApJ*, 802, L25
- Wang, P., Libeskind, N. I., Pawłowski, M. S., et al. 2021, *arXiv e-prints*, arXiv:2104.12787
- Westmeier, T., Obreschkow, D., Calabretta, M., et al. 2017, *MNRAS*, 472, 4832
- Willman, B., Dalcanton, J. J., Martínez-Delgado, D., et al. 2005, *ApJ*, 626, L85
- Wright, E. L., Eisenhardt, P. R. M., Mainzer, A. K., et al. 2010, *AJ*, 140, 1868
- Zou, H., Zhou, X., Fan, X., et al. 2019, *ApJS*, 245, 4
- Zucker, D. B., Belokurov, V., Evans, N. W., et al. 2006, *ApJ*, 650, L41